Self-Assembly of MXene-Surfactants at Liquid–Liquid Interfaces: From Structured Liquids to 3D Aerogels

Shaowei Shi[+], Bingqing Qian[+], Xinyu Wu, Huilou Sun, Haiqiao Wang, Hao-Bin Zhang,* Zhong-Zhen Yu, and Thomas P. Russell**

Abstract: 2D transition metal carbides and nitrides (MXenes), a class of emerging nanomaterials with intriguing properties, have attracted significant attention in recent years. However, owing to the highly hydrophilic nature of MXene nanosheets, assembly strategies of MXene at liquid–liquid interfaces have been very limited and challenging. Herein, through the cooperative assembly of MXene and amine-functionalized polyhedral oligomeric silsesquioxane at the oil–water interface, we report the formation, assembly, and jamming of a new type MXene-based Janus-like nanoparticle surfactants, termed MXene-surfactants (MXSs), which can significantly enhance the interfacial activity of MXene nanosheets. More impor- tantly, this simple assembly strategy opens a new platform for the fabrication of functional MXene assemblies from meso- scale (e.g., structured liquids) to macroscale (e.g., aerogels), that can be used for a range of applications, including nanocomposites, electronic devices, and all-liquid microfluidic devices.

Interfacial assembly between two immiscible liquids has been recognized as one of the most powerful techniques to integrate various nanoparticle (NP) building blocks into mesoscale (e.g., colloidosomes) or macroscale constructs (e.g., thin films and foams), in which the intriguing optical, magnetic, and electronic properties at the nanoscale can be integrated into the resultant assemblies.[1–3] The reduction of the Helmholtz free energy is the main driving force for the segregation of NPs to the interface.[4] However, in comparison to micrometer-sized colloidal particles, the reduction in the interfacial energy per NPs is much smaller. As a result, the assembly of NPs at liquid–liquid interfaces is usually dynamic and size-dependent, coexisting with adsorption and desorption processes, leading to an instability of NP assemblies.[5,6] To enhance the interfacial activity of NPs, recently, an alternative strategy was enabled by the interactions between NPs and oligomeric/polymeric ligands at the oil-water interface.[7] Here, the NPs and ligands, having complementary functionality, interact with one another only at the interface and form nanoparticle surfactants (NPSs) in situ, rendering the NPs irreversibly bound to the interface. If a biphasic system stabilized by NPSs is perturbed by an external field (e.g., electric or shear), the interfacial area increases, leading to the formation and assembly of more NPSs at the extra interfaces. Upon removal of the external field, the interfacial area decreases to reduce the free energy, compressing the NPS assemblies and jamming the NPSs at the interface. This arrests any further change in the interfacial area, locking in highly non-equilibrium shapes of one liquid in the second.[8–12] These so-called “structured liquids” are reconfigurable, since the assemblies can be un-jammed and the liquids re-shaped, and responsive owing to the interactions between the NPs and ligands and, also, chemical functionality incorporated into either. Consequently, the assemblies can adapt to their environs. Such structured liquids open a simple, universal pathway for the interfacial self-assembly of NPs of different size, shape, and chemical constitution and for the fabrication of hierarchical assemblies that can evolve response to environmental changes.[13–16]

MXenes, an emerging new family of two-dimensional (2D) early transition metal carbides and nitrides, have gained increasing attention since their first discovery in 2011.[17] MXenes are generally produced by selectively etching the A layers from their MAX phases, where M is an early transition metal, A is mainly a group IIIA or IVA element, and X is carbon and/or nitrogen. The obtained MXenes through exfoliation of their corresponding MAX phases can be represented by a general formula of $M_{n+1}X_nT_x$, where T_x refers to the surface functional groups (OH, O, and/or F) and n = 1, 2, or 3. As a graphene-like 2D material, the distinctive properties of MXenes, especially the high hydrophilicity and metallic conductivity, make them attractive for many appli- cations, such as energy storage, sensors, catalysis, nanocom- posites, and electromagnetic interference (EMI) shield-[18, 19]

[*] Prof. S. Shi,[+] B. Qian,[+] H. Sun, Prof. T. P. Russell
Beijing Advanced Innovation Center for Soft Matter Science and Engineering, Beijing University of Chemical Technology
Beijing 100029 (China)
E-mail:
shisw@mail.buct.edu.cn
russell@mail.pse.umass.edu
X. Wu, Prof. H. Wang, Prof. H.-B. Zhang, Prof. Z.-Z. Yu State Key Laboratory of Organic-Inorganic Composites Beijing University of Chemical Technology
Beijing 100029 (China)
E-mail:
zhanghaobin@mail.buct.edu.cn Prof.
T. P. Russell
Department of Polymer Science and Engineering
University of Massachusetts
Amherst, MA 01003 (USA)
and
Materials Sciences Division, Lawrence Berkeley National Laboratory 1 Cyclotron Road, Berkeley, CA 94720 (USA)

[+] These authors contributed equally to this work.

ing Up to now, applications of MXenes as building .

blocks, functional assemblies including one-dimensional (1D) fibers,[20–22] 2D films,[23–27] and 3D monoliths[28–32] have been reported through a variety of assembly strategies. However,

despite such progress, little attention has been paid to the interfacial properties of MXenes between two immiscible liquids (e.g., oil and water), and the construction of functional assemblies by the interfacial self-assembly of MXenes is still limited. The inherent negative charge of the oil–water interface is the primary reason underpinning this. Pristine MXenes are negatively charged and strongly hydrophilic and, as such will not segregate to the interface, but remain dispersed in the aqueous phase. Very recently, by the electro- static adsorption of cationic cetyltrimethylammonium bromide (CTAB) onto the MXene surface, Huang and co- workers reported that the hydrophilic–hydrophobic balance of MXene could be tuned, and stable Pickering emulsions could be prepared. Subsequently, 3D porous architectures could be achieved by polymerizing the continuous phase.[33] This approach, though, requires careful surface modification and strict control of reaction conditions. In addition, the polymerization usually leaves residual catalysis and unreacted monomers in the framework, which can significantly influ- ence the performance of the resultant assemblies.

In this work, we use $Ti_3C_2T_x$, the most widely studied MXene, and oil-soluble amine-functionalized polyhedral oligomeric silsesquioxane (POSS-NH_2, Figure S1) as model materials to investigate the formation, assembly, and jamming of a new MXene-based NPS, termed MXene-surfactant (MXS), at the oil–water interface. By the cooperative assembly of $Ti_3C_2T_x$ and POSS-NH_2, MXSs form rapidly at the liquid–liquid interface, assemble into a layer consisting of overlapping MXene nanosheets, and when jammed, offer a robust assembly with excellent mechanical properties. Interestingly, by tuning the concentration of POSS-NH_2 in the oil phase, the degree of overlap of the MXene nanosheets can be effectively manipulated, leading to a tunability of the MXS assemblies. Using concentrated Pickering emulsions as the templates, lightweight, hydrophobic, isotropic MXene aerogels with excellent mechanical properties can be easily prepared by one-step freeze-drying, where the pore size and shape are commensurate with those of the emulsion droplets (Figure 1). Furthermore, the oil absorption capacity of the as- prepared MXene aerogels and the EMI shielding perfor- mance of MXene@epoxy nanocomposites are explored, where both of them show promising results.

The kinetics of the MXS formation and assembly at the oil–water interface was probed by tracking the dynamic surfactants.

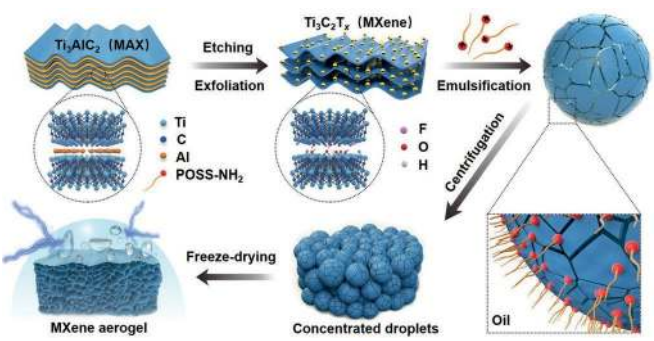

Figure 1. Schematic showing the construction of Pickering emulsions and MXene aerogels by using MXene

interfaical tension (g) using pendant drop tensiometry. For all measurments in this work, the pH value of the aqueous phase is fixed at 5.0, to ensure that MXene is well dispersed. As shown in Figure 2 a,b, with $Ti_3C_2T_x$ dispersed in water while

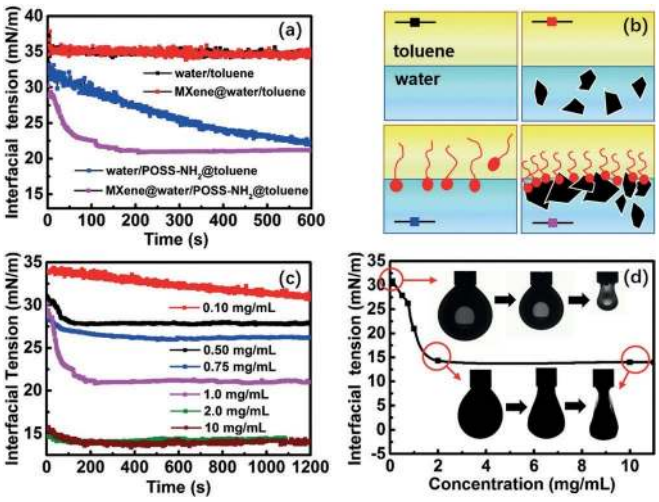

Figure 2. a) Time evolution of interfacial tension of different oil–water systems including water/toluene, MXene@water/toluene, water/POSS- NH_2@toluene, and MXene@water/POSS-NH_2@toluene, [$Ti_3C_2T_x$] = 1.0 mgmL$^{@1}$, [POSS-NH_2] = 1.0 mgmL$^{@1}$. b) Schematics of different oil-water systems in (a). c) Time evolution of interfacial tension with different MXene concentrations, [POSS-NH_2] = 1.0 mgmL$^{@1}$. d) Equilibrium interfacial intension of (c) and jamming behavior at different MXene concentrations of 0.10, 2.0, and 10 mgmL$^{@1}$.

the oil phase is pure toluene, the equilibrium interfacial tension is circa 35 mn m$^{@1}$, which is almost the same as that of the pure water–toluene system (g & 35 mn m$^{@1}$), indicating that the as-received $Ti_3C_2T_x$ is not interfacially active. With POSS-NH_2 dissolved in toluene against a pure water phase, the interfacial tension gradually decreases from 33 to 23 mn m$^{@1}$ in 10 min, and approaches an equilibrium value over an extended period of time, indicating that POSS-NH_2 behaves as a surfactant and assembles at the oil–water interface. This also changes the charge at the interface from being negative to positive. With $Ti_3C_2T_x$ dispersed in water and POSS-NH_2 dissolved in toluene, a rapid reduction in the interfacial tension is observed in the initial 100 s and an equilibrium interfacial tension of circa 21 mn m$^{@1}$ is achieved within 250 s, showing that $Ti_3C_2T_x$ and POSS-NH_2 have interacted at the interface, significantly reducing the inter- facial tension. At equilibrium, buckling of the droplet surface can be observed when the droplet volume is decreased, confirming the formation, assembly and jamming of MXSs at the interface (Video S1). This cooperative assembly process can be described using the reported kinetic model of graphene oxide (GO) nanosheets and diblock copoly- mers,[34,35] that is, for the system with $Ti_3C_2T_x$ concentration of 1.0 mgmL$^{@1}$ and POSS-NH_2 concentration of 1.0 mgmL$^{@1}$, as $Ti_3C_2T_x$ continuously adsorbs to the interface, a random loose packing state of MXSs forms initially, behaving like an elastic film. As the adsorption of $Ti_3C_2T_x$ to the interface

continues, however, at a much slower speed, a more solid-like elastic film forms.

By increasing the $Ti_3C_2T_x$ concentration from 0.10 to 2.0 mgmL$^{@1}$ ([POSS-NH_2] = 1.0 mgmL$^{@1}$), the initial reduc- tion rate in the interfacial tension is more rapid, and the equilibrium interfacial tension decreases gradually from circa 33 to circa 13 mn m$^{@1}$, indicating that more MXSs form and assemble at the interface (Figure 2 c,d). However, when the $Ti_3C_2T_x$ concentration is greater than 2.0 mg mL$^{@1}$, no signifi- cant change is observed in the equilibrium interfacial tension (ca. 14 mn m$^{@1}$), indicating that no further adsorption of $Ti_3C_2T_x$ occurs. This is reflected in the buckling behavior when the concentrations of $Ti_3C_2T_x$ are 0.10 and 2.0 mgmL$^{@1}$, respectively. For both systems, the pendant droplet is equilibrated for 10 min before reducing the volume. As shown in Figure 2d and Video S2, in the case of [$Ti_3C_2T_x$] = 0.10 mg mL$^{@1}$, wrinkles are observed only at large areal compressions, showing that MXSs are loosely packed at the interface. When the $Ti_3C_2T_x$ concentration is 2.0 mgmL$^{@1}$, wrinkling is observed at very small compressions (Video S3), suggesting a more solid-like nature of the assembly. It should be noted that, at higher $Ti_3C_2T_x$ concentration, it is difficult to observe wrinkles at the interface since the droplet is black. However, the unusual deformation of the droplet outline during the compression demonstrates the interfacial jamming of the MXSs (Figure 2d and Figure S2). With further compression, an interfacial film can be clearly observed. Similar jamming behavior is also obtained with higher $Ti_3C_2T_x$ concentration up to 10 mg mL$^{@1}$, with a more rapid formation rate of the interfacial film (Videos S4 and S5).

Vigorously homogenizing the mixture of water with dispersed $Ti_3C_2T_x$ and oil with dissolved POSS-NH_2 resulted in the formation of stable water-in-oil (w/o) Pickering emulsions at a water/oil ratio of 1:8. Unlike conventional Pickering emulsions with spherical shapes, all the droplets in Figure 3 exhibit highly irregular shapes over a $Ti_3C_2T_x$ con-

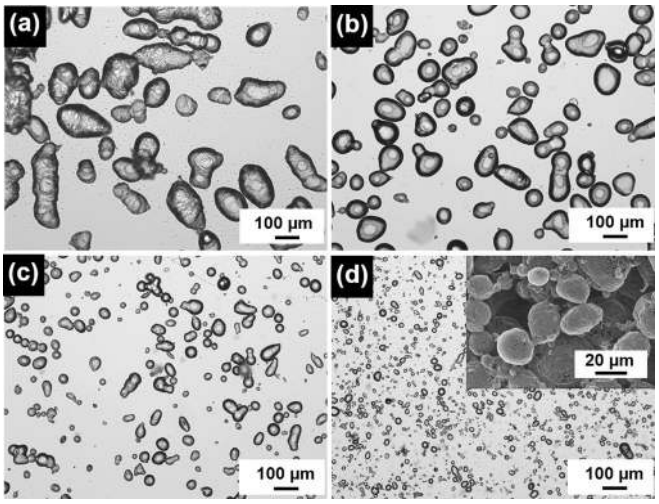

Figure 3. Optical microscopy images of emulsions droplets at different MXene concentrations of a) 0.5 mg mL$^{@1}$, b) 1.0 mg mL$^{@1}$,
c) 2.0 mgmL$^{@1}$, and d) 5.0 mgmL$^{@1}$; the inset SEM image in (d) shows the freeze-drying emulsion droplets at 5.0 mgmL$^{@1}$ of MXene; [POSS- NH_2] = 1.0 mgmL$^{@1}$.

centration range of 0.50–5.0 mg mL$^{@1}$ ([POSS-NH_2] = 1.0 mgmL$^{@1}$), which can be attributed to the very rapid interfacial jamming of the MXSs once the shearing force is removed. With an increase in the $Ti_3C_2T_x$ concentration, the droplet size decreases from several hundred microns to circa 25 mm, indicating that more interfaces are formed and are stabilized. The structure of the dried droplets in air, charac- terized using scanning electron microscopy (SEM) and optical microscopy clearly demonstrates that the droplets are encap- sulated with a thin, robust film (Figure S3). Additionally, after removing the liquid phases by freeze-drying, self-supporting, hollow $Ti_3C_2T_x$ spheres are obtained, and the structured droplets are well-preserved (Figure 3d and Figure S3 c,d).

We investigated the effect of POSS-NH_2 concentration on the morphology of the emulsion droplets (Figure 4, [$Ti_3C_2T_x$] = 1.0 mg mL$^{@1}$). With increasing POSS-NH_2 concen- tration, the irregular shapes of emulsion droplets gradually

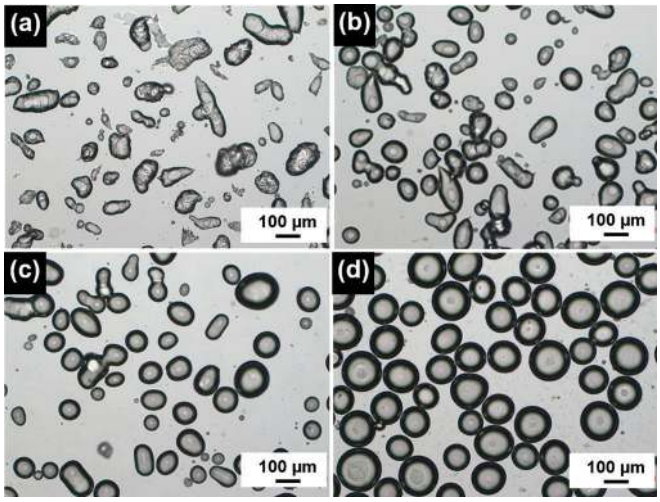

Figure 4. Optical microscopy images of emulsions droplets at different POSS-NH_2 concentrations of a) 0.10 mgmL$^{@1}$, b) 1.0 mgmL$^{@1}$,
c) 2.0 mgmL$^{@1}$, and d) 5.0 mgmL$^{@1}$. [$Ti_3C_2T_x$] = 1.0 mgmL$^{@1}$.

decrease, becoming more spherical. To explain this behavior, we measured the interfacial tension of systems with different POSS-NH_2 concentrations. As shown in Figure S4, the equilibrium interfacial tension decreases with increasing POSS-NH_2 concentration, which is consistent with systems having only POSS-NH_2 dissolved in the oil phase. However, during the extraction process, system with a higher POSS- NH_2 concentration of 5.0 mg mL$^{@1}$ shows an extremely differ- ent behavior compared to system with a low POSS-NH_2 concentration of 0.10 mg mL$^{@1}$, where the droplet detaches from the needle rather than the volume or interfacial area decreasing (Figure 5a and Videos S6 and S7). This suggests that, at low POSS-NH_2 concentrations, the adsorption rate of $Ti_3C_2T_x$ to the interface is slow, leading to a relatively loose packing of nanosheets with a low degree of overlap. When jammed, the sliding of $Ti_3C_2T_x$ is slight and the resultant solid- like film can be locked in easily. At high POSS-NH_2 concentrations, $Ti_3C_2T_x$ adsorbs to the interface very rapidly, forming a densely packed assemblies with a high overlap

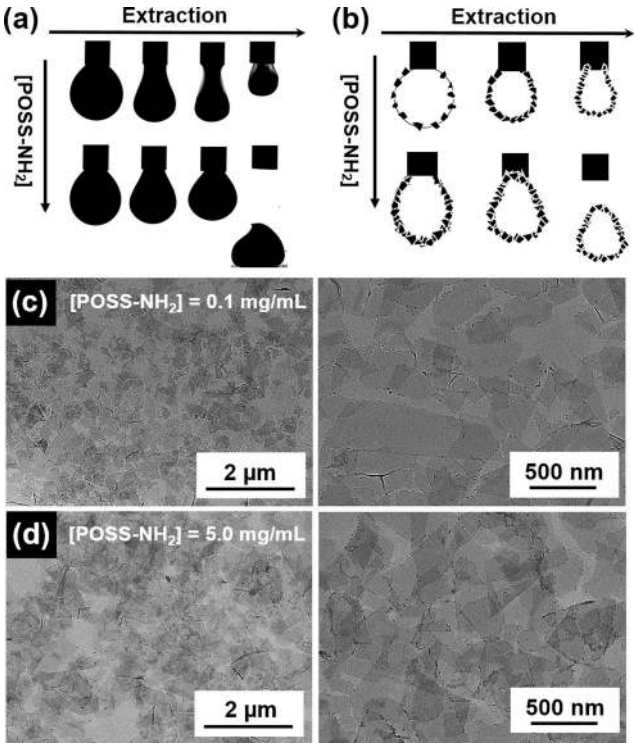

Figure 5. a) The images of the deformation and wrinkle behavior of the droplets at different POSS-NH_2 concentrations of 0.10 $mgmL^{@1}$ (top) and 5.0 $mgmL^{@1}$ (bottom). b) Schematics of the assembly of MXene surfactants at the interface during the extraction process at different POSS-NH_2 concentrations of 0.10 $mgmL^{@1}$ (top) and 5.0 $mgmL^{@1}$ (bottom). c,d) TEM images of the 2D MXene films with different POSS-NH_2 concentrations (the right image is the close-up view of the left image); [$Ti_3C_2T_x$] = 1.0 $mgmL^{@1}$.

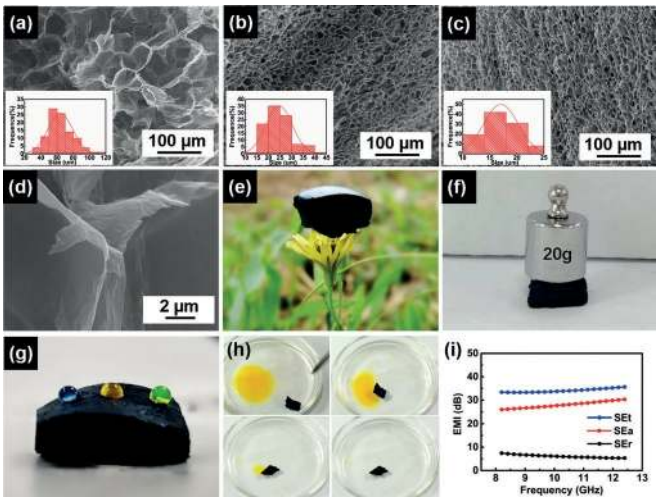

Figure 6. a–c) SEM images of MXene aerogels prepared from emul- sion templates with different MXene concentrations of a) 2.0, b) 5.0, and c) 10 $mgmL^{@1}$, [POSS-NH_2] = 1.0 mg $mL^{@1}$; d) close-up view of (c). e) A small piece of MXene aerogel on a flower; f)a small piece of aerogel (ca. 6.4 mg) supporting a 20g weight; g) water droplets on surface of MXene aerogel; h) oil absorption of MXene aerogel (the yellow oil phase is *n*-hexene dissolving azobenzene). i) EMI shielding performance of $Ti_3C_2T_x$@epoxy nanocomposite. Aerogels used in (e)–(i) are prepared in the case of [$Ti_3C_2T_x$] = 10 $mgmL^{@1}$ and [POSS- NH_2] = 1.0 $mgmL^{@1}$.

degree. Owing to the negatively-charged surface of $Ti_3C_2T_x$, at the jamming transition, the repulsion between overlapped $Ti_3C_2T_x$ nanosheets results in a sliding in the direction of needle outlet, leading to an concentration of nanosheets at the needle outlet, inhibiting the further extraction of droplet, causing a detachment of the droplet (Figure 5 b). For the structured emulsions, this sliding behavior will lead to a shape transition from highly a non-equilibrium state to the more equilibrium state. In support of this argument, 2D films were prepared with different POSS-NH_2 concentrations and characterized by transmission electron microscope (TEM). As shown in Figure 5 c,d, at higher POSS-NH_2 concentrations, the degree of the $Ti_3C_2T_x$ nanosheets overlap is more obvious. Having achieved this level of interfacial control, MXene aerogels were fabricated by freeze-drying the concentrated emulsion droplets stabilized by MXSs. A detailed description of the aerogel preparation can be found in the Supporting Information, Experimental Section. As shown in Figure 6 a–c, by using emulsion templates of different size, the pore structure of the corresponding aerogels can be effectively tuned from circa 60 to circa 15 mm. Owing to the dense packing of the MXSs at the interface, the integrity of the emulsion templates is well-preserved, which is crucial for the construction of robust and conductive 3D frameworks (Fig- ure 6 d). In the case of aerogels with circa 15 mm pores, the average density is 12.8 $mgcm^{@3}$ and a 20 g weight can be supported with negligible deformation (the weight of aerogel used here is 6.4 mg), indicating the excellent mechanical strength of the lightweight aerogel (Figure 6 e,f). A Si peak (103 eV) in the X-ray photoelectron spectroscopy (XPS) and Si@O/C@H peaks (1091.2/2923 $cm^{@1}$) in the Fourier transform infrared (FTIR) spectroscopy demonstrate the successful integration of POSS-NH_2 into the MXene aerogel (Figures S5 and S6). Figure S7 shows the comparison of X-ray diffraction (XRD) patterns for a compact $Ti_3C_2T_x$ film and the as- fabricated 3D $Ti_3C_2T_x$ aerogel. Characteristic (002) peak for MXene aerogel is observed at 2q = 7.128, which is at a slightly larger angle than that of MXene film (6.568). This corresponds to an decrease in the interlayer spacing in MXene aerogel from 1.34 to 1.24 nm owing to the elimination of H_2O between the layers during the freeze-drying process.[28] The gravimetric analysis (TGA) analysis of the POSS-NH_2 and MXene aerogel shows that when the temperature is above 500 **8**C, POSS-NH_2 completely degrades with about 15 % weight lost, indicating that the mass ratio of POSS-NH_2: $Ti_3C_2T_x$ is circa 1:6 (Figure S8).

The surface wetting behavior of the aerogel was inves- tigated by measuring the water contact angle. For pure MXene film, owing to the oxygen and fluorine terminal groups on the MXene surface, it is hydrophilic with a contact angle of 42**8** (Figure S9 a). For the as-prepared MXene aerogel, a large water contact angle of 1238 is observed, indicating the hydrophobic nature of this construction due to the attachment of hydrophobic POSS-NH_2 on the MXene surface (Figure 6g and Figure S9 b). In a previous study, we have reported the first hydrophobic 2D MXene films by

a hydrazine-induced foaming process.[26] However, to our knowledge, there is no report on hydrophobic 3D MXene aerogels. This hydrophobicity and porous structure make the MXene aerogel a promising candidate for selectively absorb- ing organic solvents such as toluene, *n*-hexene and silicon oil (Figure 6 h, Figure S10, and Video S8). For example,a toluene absorption of up to 9000 % is found, much higher than literature values.[30]

Finally, by taking advantage of the conductive nature of the MXene aerogel (electrical conductivity is ca. 376 S $m^{@1}$), we fabricated the $Ti_3C_2T_x$@epoxy nanocomposites by directly filling epoxy precursor into MXene aerogels. The 3D conductive network is preserved in the epoxy matrix with an electrical conductivity of 195.3 S $m^{@1}$. EMI shielding measurements, including total shielding effectiveness (SEt), absorption shielding effectiveness (SEa), and reflection shielding effectiveness (SEr) of the as-prepared $Ti_3C_2T_x$@epoxy nanocomposites are shown in Figure 6 i, indicating that EMI shielding performance is mainly due to the absorption of electromagnetic waves within the material. The nanocomposite with 0.40 vol% of $Ti_3C_2T_x$ exhibits a superb average EMI shielding performance of 34.5 dB over the whole X-band, which is sufficient for many civil and military applications. The results of SE divided by sample thickness (SE/*d*) are summarized in Figure S11 and Table S1 to eliminate the effect of specimen thickness. It is worth noting that the as-prepared $Ti_3C_2T_x$@epoxy nanocomposite shows a competitive shielding performance of 17.3 $dBmm^{@1}$ in comparison to other shielding materials.[32]

In summary, we have demonstrated the interfacial activity of MXSs formed by the interactions between $Ti_3C_2T_x$ and POSS-NH_2 at the oil–water interface. MXSs rapidly form and assemble at the interface with a controllable packing density, and when jammed, produce a solid-like assembly with excellent mechanical properties. Taking advantage of MXSs, 2D films, and structured Pickering emulsions can be easily prepared. Furthermore, by freeze-drying the concentrated emulsion droplets, lightweight, hydrophobic 3D MXene aerogels are produced from the bottom up, which can be used for oil adsorption and EMI shielding. This intriguing assembly strategy at the liquid–liquid interface provides a simple route to construct MXene assemblies from the mesoscale to macroscale, having significant practical importance.

Acknowledgements

This work was supported by the National Natural Science Foundation of China (51903011, 51922020), the Beijing Natural Science Foundation (2194083). T.P.R. was supported by the U.S. Department of Energy, Office of Science, Office of Basic Energy Sciences, Materials Sciences and Engineering Division under Contract No. DE-AC02-05-CH11231 within the Adaptive Interfacial Assemblies Towards Structuring Liquids program (KCTR16)

[1] S. Shi, T. P. Russell, *Adv. Mater.* 2018, *30*, 1800714.
[2] J. Forth, P. Y. Kim, G. Xie, X. Liu, B. A. Helms, T. P. Russell, *Adv. Mater.* 2019, *31*, 1806370.
[3] A. Bçker, J. He, T. Emrick, T. P. Russell, *Soft Matter* 2007, *3*, 1231 – 1248.
[4] P. Pieranski, *Phys. Rev. Lett.* 1980, *45*, 569 – 572.
[5] B. P. Binks, *Curr. Opin. Colloid Interface Sci.* 2002, *7*, 21–41.
[6] R. Aveyard, B. P. Binks, J. H. Clint, *Adv. Colloid Interface Sci.* 2003, *100 – 102*, 503 – 546.
[7] M. M. Cui, T. Emrick, T. P. Russell, *Science* 2013, *342*, 460 – 463.
[8] X. Liu, S. Shi, Y. Li, J. Forth, D. Wang, T. P. Russell, *Angew. Chem. Int. Ed.* 2017, *56*, 12594 – 12598; *Angew. Chem.* 2017, *129*, 12768 – 12772.
[9] S. Shi, X. Liu, Y. Li, X. Wu, D. Wang, J. Forth, T. P. Russell, *Adv. Mater.* 2018, *30*, 1705800.
[10] Y. Li, X. Liu, Z. Zhang, S. Zhao, G. Tian, J. Zheng, D. Wang, S. Shi, T. P. Russell, *Angew. Chem. Int. Ed.* 2018, *57*, 13560; *Angew. Chem.* 2018, *130*, 13748.
[11] A. Toor, B. A. Helms, T. P. Russell, *Nano Lett.* 2017, *17*, 3119 – 3125.
[12] C. Huang, Z. Sun, M. Cui, F. Liu, B. A. Helms, T. P. Russell, *Adv. Mater.* 2016, *28*, 6612 – 6618.
[13] C. Huang, J. Forth, W. Wang, K. Hong, G. S. Smith, B. A. Helms, T. P. Russell, *Nat. Nanotechnol.* 2017, *12*, 1060 – 1063.
[14] J. Forth, X. Liu, J. Hasnain, A. Toor, K. Miszta, S. Shi, P. L. Geissler, T. Emrick, B. A. Helms, T. P. Russell, *Adv. Mater.* 2018, *30*, 1707603.
[15] A. Toor, S. Lamb, B. A. Helms, T. P. Russell, *ACS Nano* 2018, *12*, 2365 – 2372.
[16] W. Feng, Y. Chai, J. Forth, P. D. Ashby, T. P. Russell, B. A. Helms, *Nat. Commun.* 2019, *10*, 1095.
[17] M. Naguib, M. Kurtoglu, V. Presser, J. Lu, J. Niu, M. Heon, L. Hultman, Y. Gogotsi, M. W. Barsoum, *Adv. Mater.* 2011, *23*, 4248 – 4253.
[18] M. Naguib, V. N. Mochalin, M. W. Barsoum, Y. Gogotsi, *Adv. Mater.* 2014, *26*, 992 – 1005.
[19] D. Xiong, X. Li, Z. Bai, S. Lu, *Small* 2018, *14*, 1703419.
[20] M. Hu, Z. Li, G. Li, T. Hu, C. Zhang, X. Wang, *Adv. Mater. Technol.* 2017, *2*, 1700143.
[21] K. Krishnamoorthy, P. Pazhamalai, S. Sahoo, S.-J. Kim, *J. Mater. Chem. A* 2017, *5*, 5726 – 5736.
[22] Q. Yang, Z. Xu, B. Fang, T. Huang, S. Cai, H. Chen, Y. Liu, K. Gopalsamy, W. Gao, C. Gao, *J. Mater. Chem. A* 2017, *5*, 22113 – 22119.
[23] Z. Ling, C. E. Ren, M. Q. Zhao, J. Yang, J. M. Giammarco, J. Qiu, M. W. Barsoum, Y. Gogotsi, *Proc. Natl. Acad. Sci. USA* 2014, *111*, 16676 – 16681.
[24] A. D. Dillon, M. J. Ghidiu, A. L. Krick, J. Griggs, S. J. May, Y. Gogotsi, M. W. Barsoum, A. T. Fafarman, *Adv. Funct. Mater.* 2016, *26*, 4162 – 4168.
[25] L. Ding, Y. Wei, Y. Wang, H. Chen, J. Caro, H. Wang, *Angew. Chem. Int. Ed.* 2017, *56*, 1825 – 1829; *Angew. Chem.* 2017, *129*, 1851 – 1855.
[26] J. Liu, H. B. Zhang, R. Sun, Y. Liu, Z. Liu, A. Zhou, Z. Z. Yu, *Adv. Mater.* 2017, *29*, 1702367.

[27] M. Q. Zhao, X. Xie, C. E. Ren, T. Makaryan, B. Anasori, G. Wang, Y. Gogotsi, *Adv. Mater.* 2017, *29*, 1702410.
[28] L. Li, M. Zhang, X. Zhang, Z. Zhang, *J. Power Sources* 2017, *364*, 234 – 241.
[29] Y. Jiang, X. Xie, Y. Chen, Y. Liu, R. Yang, G. Sui, *J. Mater. Chem. C* 2018, *6*, 8679 – 8687.
[30] R. Bian, G. He, W. Zhi, S. Xiang, T. Wang, D. Cai, *J. Mater. Chem. C* 2019, *7*, 474 – 478.
[31] J. Liu, H. B. Zhang, X. Xie, R. Yang, Z. Liu, Y. Liu, Z. Z. Yu, *Small* 2018, *14*, 1802479.
[32] S. Zhao, H. B. Zhang, J. Q. Luo, Q. W. Wang, B. Xu, S. Hong, Z. Z. Yu, *ACS Nano* 2018, *12*, 11193 – 11202.
[33] R. Bian, R. Lin, G. Wang, G. Lu, W. Zhi, S. Xiang, T. Wang, P. S. Clegg, D. Cai, W. Huang, *Nanoscale* 2018, *10*, 3621 – 3625.
[34] Z. Sun, T. Feng, T. P. Russell, *Langmuir* 2013, *29*, 13407 – 13413.
[35] D. Chen, Z. Sun, T. P. Russell, L. Jin, *Langmuir* 2017, *33*, 8961 – 8969.